Masanori Tomonari, Kiyonobu Ida, Hiromi Yamashita, and Tetsu Yonezawa	Size-controlled Oxidation Resistant Copper Fine Particles Covered by Biopolymer Nanoskin	J. Nanosci. Nanotech.	8(5)	2468-2471	2008
米澤　徹	金属ナノ粒子の湿式合成とその応用	ケミカルエンジニヤリング.	53(8)	583-587	2008
Tetsu Yonezawa, Yoshinori Yamanoi, and Hiroshi Nishihara	Cross-sectional STEM Observation of Nanoparticle-Attached Silicon Wafer: Specimen Prepared by Focused Ion-Beam	J. Nanosci. Nanotech.	8(3)	1518-1522	2008
Tetsu Yonezawa, Keigo Kamoshita, Masayoshi Tanaka, and Takatoshi Kinoshita	Easy Preparation of Stable Iron Oxide Nanoparticles using Gelatin as Stabilizing Molecules	Jpn. J. Appl. Phys.	47(2)	1389-1392	2008
Mariko Miyachi, Makiko Ohta, Misaki Nakai, Yoshihiro Kubota, Yoshinori Yamanoi, Tetsu Yonezawa, and Hiroshi Nishihara	Surface Bottom-up Fabrication of Porphyrin-terminated Metal Complex Molecular Wires with Photo-electron Conversion Properties on ITO	Chem. Lett.	27(4)	404-405	2008
Tetsu Yonezawa, Shinsuke Takeoka, Hiroshi Kishi, Kiyonobu Ida, and Masanori Tomonari	Preparation of Copper Fine Particle Paste and Application of This Paste as Material of Inner Electrodes of Multilayered Ceramic Capacitor (MLCC)	Nanotechnology	19	145706/1-5	2008
Tetsu Yonezawa, Hideya Kawasaki, Akira Tarui, Takehiro Watanabe, Ryuichi Arakawa, Toshihiro Shimada, Fumitaka Mafune	Detailed Investigation on the Possibility of Various Metal Elements for Surface-Assisted Laser Desorption/ Ionization Mass Spectrometry	Anal. Sci.	25(3)	339-346	2009
Nao Terasaki, Noritaka Yamamoto, Takashi Hiraga, Yoshinori Yamanoi, Tetsu Yonezawa, Hiroshi Nishihara, Tsutomu Ohmori, Makoto Sakai, Masaaki Fujii, Akihiro Tohri, Masako Iwai, Yasunori Inoue, Satoshi Yoneyama, Makoto Minakata, and Isao Enami	Plugging a Molecular Wire into Photosystem I for Reconstitution of the Photoelectric Conversion System on a Gold Electrode	Angew. Chem. Int. Ed.		in press.	2009
Mariko Miyachi, Yoshinori Yamanoi, Tetsu Yonezawa, Hiroshi Nishihara, Michinao Iwai, Masae Konno, Masako Iwai, and Yasunori Inoue	Surface Immobilization of PSI Using Vitamin K_1-like Molecular Wires for Fabrication of a Bio-photoelectrode	J. Nanosci. Nanotech.		in press.	2009
Akira Tarui, Hideya Kawasaki, Takuma Taiko, Takehiro Watanabe, Tetsu Yonezawa, and Ryuichi Arakawa	Aggregated gold-nanoparticle-supported silicon plate with cationic diblock copolymer micelles for surface-assisted laser desorption/ionization mass spectrometry of peptides	J. Nanosci. Nanotech.		in press.	2009
Uo M., Asakura K., Tamura K., Totsuka Y., Abe S., Akasaka T., and Watari F.	XAFS analysis of Ti and Ni dissolution from pure Ti, Ni-Ti alloy, and SUS304 in soft tissues,	*Chem. Lett.*,	37,	958-959,	2008
R. J. Joseyphus, K. Shinoda, Y. Sato, K. Tohji, B. Jeyadevan	Composition controlled synthesis of fcc-FePt nanoparticles using a modified polyol process	*J. Mater. Sci.*	43	2402-2406	2008

T. Arai, S. Senda, Y. Sato, H. Takahashi, K. Shinoda, B. Jeyadevan, K. Tohji	Cu-Doped ZnS Hollow Particle with High Activity for Hydrogen Generation from Alkaline Sulfide Solution under Visible Light	*Chem. Mater.*	20	1997-2000	2008
○S. Samukawa, Y. Ishikawa, K. Okumura, Y. Sato, K. Tohji, T. Ishida	Damage-free surface treatment of carbon nanotubes and self-assembled monolayer devices using a neutral beam process for fusing top-down and bottom-up processes	*J. Phys. D*	41	24006(1)-24006(6)	2008
○Y. Sato, A. Yokoyama, T. Kasai, S. Hashiguchi, M. Ootsubo, S. Ogino, N. Sashida, M. Namura, K. Motomiya, B. Jeyadevan, K. Tohji	In vivo rat subcutaneous tissue response of binder-free multi-walled carbon nanotube blocks cross-linked by de-fluorination	*Carbon*	46	1927-1934	2008
Y. Sato, K. Hasegawa, Y. Nodasaka, K. Motomiya, M. Namura, N. Ito, B. Jeyadevan, K. Tohji	Reinforcement of rubber using radial single-walled carbon nanotube soot and its shock dampening properties	*Carbon*	46	1509-1512	2008
Y. Sato, M. Ootsubo, G. Yamamoto, G. Van Lier, M. Terrones, S. Hashiguchi, H. Kimura, A. Okubo, K. Motomiya, B. Jeyadevan, T. Hashida, K Tohji	Super-robust, lightweight, conducting carbon nanotube blocks cross-linked by de-fluorination	*ACS Nano*	2	348-356	2008
○佐藤義倫	カーボンナノチューブの表面改質に関わる細胞毒性	*Material Stage*	7	98-105	2008
M. Namura, I. Waki, Y. Sato, G. Yamamoto, A. Okubo, H. Kimura, N. Osaka, K. Motomiya, T. Hashida, B. Jeyadevan, K. Tohji	Preparation and characterization of lanthanum carbide encapsulated carbon nanocapsules soot / lanthanum hexaboride nanocomposites	*Mater. Lett.*	in press		2009
○名村 優、佐藤義倫、田路和幸	カーボンナノチューブの長さ制御	*粉体技術*	1	44-50	2009
平田　恵理	カーボンナノチューブコートしたコラーゲンスポンジの3次元培養担体への応用	DE	168	32-33	2008
○Eri Hirata,　Motohiro Uo, Hiroko Takita, Tsukasa Akasaka, Fumio Watari, Atsuro Yokoyama	Development of a 3D collagen scaffold coated with multiwalled carbon nanotubes	J Biomed Mater Res B	DOI: 10.1002/jbm.b.31327		2009
Hayashi R, Kondo E, Tohyama H, Saito T, Yasuda K.	In vivo local administration of osteogenic protein-1 increases structural properties of the overstretched anterior cruciate ligament with partial midsubstance laceration: a biomechanical study in rabbits.	J Bone Joint Surg Br.	90(10)	1392-400.	2008
Tohyama S, Onodera S, Tohyama H, Yasuda K, Nishihira J, Mizue Y, Hamasaka A, Abe R, Koyama Y.	A novel DNA vaccine-targeting macrophage migration inhibitory factor improves the survival of mice with sepsis.	Gene Ther	15(23)	1513-22	2008
Hayashi R, Kitamura N, Kondo E, Anaguchi Y, Tohyama H, Yasuda K.	Simultaneous anterior and posterior cruciate ligament reconstruction in chronic knee instabilities: surgical concepts and clinical outcome.	Knee Surg Sports Traumatol Arthrosc.	16(8)	763-9.	2008

Onodera S, Oshima S, Nishihira J, Yasuda K, Tohyama H, Irie K, Koyama Y.	Active immunization against macrophage migration inhibitory factor using a novel DNA vaccine prevents ovariectomy-induced bone loss in mice.	Vaccine	26(6)	829-36	2008
Miyatake S, Tohyama H, Kondo E, Katsura T, Onodera S, Yasuda K.	Local administration of interleukin-1 receptor antagonist inhibits deterioration of mechanical properties of the stress-shielded patellar tendon.	J Biomech	41(4)	884-9	2008
Okamoto S, Tohyama H, Kondo E, Anaguchi Y, Onodera S, Hayashi K, Yasuda K.	Ex vivo supplementation of TGF-beta1 enhances the fibrous tissue regeneration effect of synovium-derived fibroblast transplantation in a tendon defect: a biomechanical study.	Knee Surg Sports Traumatol Arthrosc.	16(3)	333-9.	2008
Tomita M, Yokoyama K, Asaoka K, Sakai J.	Hydrogen thermal desorption behavior of Ni-Ti superelastic alloy subjected to tensile deformation after hydrogen charging.	Mater Sci Eng i A	476	308-315	2008
Kitazoe K, Abe M, Hiasa M, Oda A, Amou H, Harada T, Nakano A, Takeuchi K, Hashimoto T, Ozaki S, Matsumoto T.	Valproic acid exerts anti-tumor as well as anti-angiogenic effects on myeloma.	Int J Hematol	89	45-57	2009
Horiuchi S, Kaneko K, Mori H, Kawakami E, Tsukahara T, Yamamoto K, Hamada K, Asaoka K, Tanaka E.	Enamel bonding of self-etching and phosphoric acid-etching orthodontic adhesives: Shear bond strength and enamel surface.	Dent Mater J		In press	2009
Sultana R, Hamada K, Ichikawa T, Asaoka K.	Effects of heat treatment on the bioactivity of surface-modified titanium in calcium solution.	Biomed Mater Eng		In press	2009
Hosoki M, Bando E, Asaoka K, Takeuchi H, Nishigawa K.	Assessment of allergic hypersensitivity to dental materials.	Biomed Mater Eng.		In press	2009
Horiuchi S, Asaoka K, Tanaka E.	Development of a novel cement by conversion of hopeite in set zinc phosphate cement into biocompatible apatite.	Biomed Mater Eng.		In press	2009
Asaoka K, Maejima K.	Hydrogen-related degradation of mechanical properties of titanium and titanium alloys.	J ASTM Int.		In press	2009
Sone, H., Fugetsu, B., Tsukada, T., Endo, M.	Affinity-based elimination of aromatic VOCs by highly crystalline multi-walled carbon nanotubes	Talant	74	1265-1270	2008
Yu, H., Chen, X., Tusjii, K., Fugetsu, B.	Use of ultra-thin cross-linked polymer films for preparation of stable mono-dispersed carbon nanotubes	Materials letters	62	4050-4052	2008

Fugetsu, 他6名	Electrical conductivity and electromagnetic in terference shielding efficiency of carbon nanotube/cellulose composite paper	Carbon	46	1256-1258	2008
○Fugetsu, B., Akiba, E., Hachya, M., Endo, M.	The production of soft, durable and electrically conductive polyester multifilament yarns by dye-printing them with carbon nanotubes	Carbon	47	527-5370	2009
Kondoh, K., Threrujirapapong, T., Imai, H., Umeda, J., Fugetsu, B.	CNTs/TiC reinforced titanium matrix nanocomposites via powder metallurgy and its micro-structural and mechanical properties	J.nanomaterials	2008	1-4	2009
Noriyuki Takashi, Fumio Watari, Yasunori Totsuka	Inflammatory Exudates Modulate the Function and Apoptosis of Neutrophils	Oral Science International	5 (2)	122-130	2008
Makoto Matsuoka, Tsukasa Akasaka, Takeshi Hashimoto, Yasunori Totsuka and Fumio Watari	Improvement in cell proliferation on silicone rubber by carbon nanotube coating	Bio-Medical Materials and Engineering		In press	2009
Suzuki N, Yoshimura Y, Deyama Y, Suzuki K, Kitagawa Y	Mechanical stress directly suppresses osteoclast differentiation in RAW264.7 cells	Int.J. Molecular Medicine	21	291-296	2008
J.Sato, J.Goto, T.Kato, M.Terada, A.Sato, Y.Kitagawa	Thrombocytopenia associated with loxoprofen sodium: a case report.	Asian J Oral Maxillofac surg	19	226-229	2008
Yamazaki Y, Saitoh M, Notani K, Tei K, Totsuka Y, Takinami S, Kanegae K, Inubushi M, Tamaki N, Kitagawa Y	Assessment of cervical lymph node metastases using FDG-PET in patientswith oral squamous cell carcinoma	Annals of Nuclear Medicine	22	177-184	2008
Hata H, Kitamura T, Higashino F, Hida K, Yoshida K, Ohiro Y, Totsuka Y, Kitagawa Y, Shindo M	E1AF, an ets-oncogene transcription factor expression highly correlates with malignant phenotype of malignant melan oma through upregulating membrane-type-1 matrix proteinase gene	Oncol Rep	19	1093-1098	2008
寺田典子	コラーゲン上に多層カーボンナノチューをコートした細胞培養担体の開発	DE	165	35-36	2008
○Michiko TERADA, Shigeaki ABE, Tsukasa AKASAKA, Motohiro UO, Yoshimasa KITAGAWA and Fumio WATARI	Development of a Multiwalled Carbon Nanotube Coated Collagen Dish	Dent. Mater. J.	28	82-88	2008
Michiko Terada, Shigeaki Abe, Tsukasa Akasaka, Motohiro Uo, Yoshimasa Kitagawa and Fumio Watari	Multiwalled carbon nanotube coating on titanium	Biomed Mater Eng.		in press	2009
Yoshinori Kuboki, Michiko Terada, Yoshimasa Kitagawa, Shigeaki Abe, Motohiro Uo and Fumio Watari	Interaction of collagen triple-helix with carbon nanotubes: Geometric property of rod-like molecules	Biomed Mater Eng.		in press	2009

Ichinohe N, Kuboki Y, TabataY	Bone regeneration using titanium nonwoven fabrics combined with FGF-2 release from gelatin hydrogel microspheres in rabbit defects,	Tissue Engineering	Part A, 14 (10)	1663-171	2008
Fukui N, T, Kuboki Y, Aoki H.	Bone tissue reaction of nano-hydroxyapatite /collagen composite at the early stage of implantation	Biomed Mater Eng.	18 (1)	25-33	2008
Kawakami T, Kuboki Y, Tanaka J, Hijikata S, akazawa T, Murata M, Fujisawa R, Takita H, Arisue M.	Regenerative medicine of bone and teeth – with special references to biological principles, probrems and indicators.	J Hard Tissue Biology	16 (3)	2007	95-113 .
Kazuyuki Fukushima, Mitsuhiro Enomoto, Shoji Tomizawa, Makoto Takahashi, Yoshiaki Wakabayashi, Soichiro Itoh, oshinori Kuboki, Kenichi Shinomiya	The Axonal Regeneration Across a Honeycomb Collagen Sponge Applied to the Transected Spinqal Cord.	J Med and Den Sci	55 (1)	2008	71-77
Hiroshi Masago, Yasuyuki Shibuya, Sachiko Munemoto, Junichiro Takeuchi. Masahiroumeda, Takahide Komori,Kuboki,Y.	Alveolar ridge augmentation using various bone substitutes- a web form of titanium fibers promotes rapid bone development.	Kobe J Med Sci,	53	2007	257-263
Hirata I., Okazaki M	Higher Concentrations of Fluoride Ions Dramatically Inhibit the Survival of Osteoblasts.	J Oral Tissue Engin	6	3-8	2008
Matsuura A., Kubo T., Doi K., Hayashi K., Morita K., Yokota R., Hayashi H., Hirata I. , Okazaki M., Akagawa. Y.	Bone formation ability of carbonate apatite-collagen scaffolds with different carbonate contents	Dent Mater J	2	In press	2009
Xin Lin, Shigeki Matsuya, Masaharu Nakagawa, Yoshihiro Terada, Kunio Ishikawa	Effect of molding pressure on fabrication of low-crystalline calcite block	Journal of Materials Science: Materials in Medicine	19(2)	479-484	2008
S. Ohnuki, K. Okudera, K. Hamada, T. Suda, N. Hashimoto,	Observation of Hydrogen Strange Materials by Means of Environmental Cell TEM	International Symposium on Materials Design for Infrastructures, SICE2008 proceedings	6.,	pp.49-52	2008
A. Ono, H. Sitoh, S. Ohnuki, N. Hashimoto,	Micro-lamellar Structure in Hydrogen Storage Mg-Ni Alloys	Proceeding of 9th Asia-Pacific Microscopy Conference	7		2008

IV. 研究成果の刊行物・別刷

JOURNAL OF THE ROYAL SOCIETY Interface

Material nanosizing effect on living organisms: non-specific, biointeractive, physical size effects

Fumio Watari, Noriyuki Takashi, Atsuro Yokoyama, Motohiro Uo, Tsukasa Akasaka, Yoshinori Sato, Shigeaki Abe, Yasunori Totsuka and Kazuyuki Tohji

J. R. Soc. Interface published online 8 April 2009
doi: 10.1098/rsif.2008.0488.focus

Interface focus

FirstCite e-publishing

J. R. Soc. Interface
doi:10.1098/rsif.2008.0488.focus
Published online

Material nanosizing effect on living organisms: non-specific, biointeractive, physical size effects

Fumio Watari[1,*], Noriyuki Takashi[1], Atsuro Yokoyama[1], Motohiro Uo[1], Tsukasa Akasaka[1], Yoshinori Sato[2], Shigeaki Abe[1], Yasunori Totsuka[1] and Kazuyuki Tohji[2]

[1]*Graduate School of Dental Medicine, Hokkaido University, Sapporo 060-8586, Japan*
[2]*Graduate School of Environmental Studies, Tohoku University, Sendai 980-8579, Japan*

Nanosizing effects of materials on biological organisms was investigated by biochemical cell functional tests, cell proliferation and animal implantation testing. The increase in specific surface area causes the enhancement of ionic dissolution and serious toxicity for soluble, stimulative materials. This effect originates solely from materials and enhances the same functions as those in a macroscopic size as a catalyst. There are other effects that become prominent, especially for non-soluble, biocompatible materials such as Ti. Particle size dependence showed the critical size for the transition of behaviour is at approximately 100 μm, 10 μm and 200 nm. This effect has its origin in the biological interaction process between both particles and cells/tissue. Expression of superoxide anions, cytokines tumour necrosis factor-α and interleukin-1β from neutrophils was increased with the decrease in particle size and especially pronounced below 10 μm, inducing phagocytosis to cells and inflammation of tissue, although inductively coupled plasma chemical analysis showed no dissolution from Ti particles. Below 200 nm, stimulus decreases, then particles invade into the internal body through the respiratory or digestive systems and diffuse inside the body. Although macroscopic hydroxyapatite, which exhibits excellent osteoconductivity, is not replaced with natural bone, nanoapatite composites induce both phagocytosis of composites by osteoclasts and new bone formation by osteoblasts when implanted in bone defects. The progress of this bioreaction results in the conversion of functions to bone substitution. Although macroscopic graphite is non-cell adhesive, carbon nanotubes (CNTs) are cell adhesive. The adsorption of proteins and nano-meshwork structure contribute to the excellent cell adhesion and growth on CNTs. Non-actuation of the immune system except for a few innate immunity processes gives the non-specific nature to the particle bioreaction and restricts reaction to the size-sensitive phagocytosis. Materials larger than cell size, approximately 10 μm, behave inertly, but those smaller become biointeractive and induce the intrinsic functions of living organisms. This bioreaction process causes the conversion of functions such as from biocompatibility to stimulus in Ti-abraded particles, from non-bone substitutional to bone substitutional in nanoapatite and from non-cell adhesive to cell adhesive CNTs. The insensitive nature permits nanoparticles that are less than 200 nm to slip through body defence systems and invade directly into the internal body.

Keywords: nanoparticle; phagocytosis; inflammation; internal diffusion; non-specificity; immune system

1. INTRODUCTION

1.1. Nanotechnology and biological organisms

The development of nanotechnology has a large influence on human life. Completion of genome analysis has brought the post-genome era, enabling applications for biological and medical purposes. The reactions of biological organisms to proteins and saccharides including viruses, bacteria, enzymes and pharmacological agents have been investigated in biology and medicine. For materials, the reaction to the usual cases, i.e. at the macroscopic size, is well investigated.

However, the effect of micro/nanosizing of materials onto biological organisms remains unclear. Nanosizing of materials brings in a quantum effect at less than approximately 1.5 nm and the formation of activity sites such are seen in some catalysts (figure 1). The most unambiguous and influential effect is the surface

*Author for correspondence (watari@den.hokudai.ac.jp).

One contribution to a Theme Supplement 'Japanese biomaterials'.

Received 14 November 2008
Accepted 13 March 2009

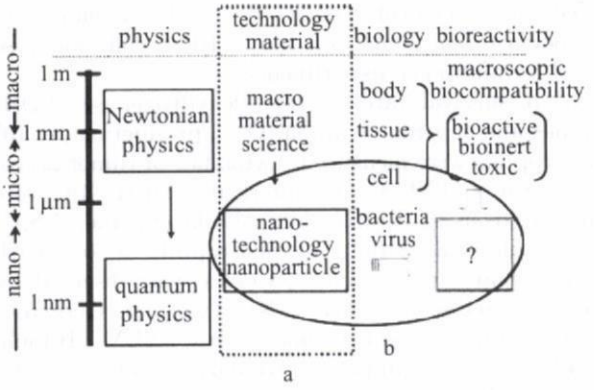

Figure 1. Correlation of the nanosizing effect with bioreactivity in relational map of nanotechnology with physics and biology. a, Specific surface area effect originated solely from material properties; b, physical size effect arising through particle–cell/tissue interaction.

area effect. It is well known that the specific surface area, which is defined as surface area for unit volume, is increased reciprocally with a decrease in particle size and chemical reactivity is pronounced. Therefore, high throughput is expected in the functions and performances of material properties and devices.

1.2. Specific surface area effect

One of the most important factors that affects the biocompatibility of materials is ionic dissolution, which is closely related to the specific surface area. This is also true for micro- and nanosizes, and very often becomes apparent as stimulus and toxicity. The nanosizing effect that affects biocompatibility is usually interpreted from this aspect.

1.3. Physical size and shape effect

On the other hand, corrosion-resistant and biocompatible Ti (Matsuno *et al.* 2001) causes inflammation, leading to osteolysis for the abraded fine particles (Tamura, Y. *et al.* 2002*a*,*b*; Uo *et al.* 2005*b*, 2007; Zhu & Watari 2007) which are produced from an artificial joint. Asbestos (Watari *et al.* 2006), a kind of clay mineral, induces mesothelioma after long-term, exposure to large quantities. These phenomena cannot be explained by the specific surface area effect and understood to be a different effect, i.e. physical size and shape effect, apart from the material properties of either toxicity or biocompatibility.

1.4. Nanoapatite

Meanwhile, hydroxyapatite (HAP), the main component of bone, shows different behaviour in synthetic apatite and bone. Synthetic HAP of a macroscopic size exhibits excellent osteoconductivity. However, it is not substituted for natural bone and remains permanently in the body. Therefore, it is used as an implant (Watari *et al.* 1997, 2004; Li *et al.* 2008*b*; Matsuo *et al.* 2001). Natural bone is composed of collagen and nanocrystallites of apatite of approximately 50 nm (Watari *et al.* 2001, 2005). Bone is continuously remodelled by resorption and new bone formation. Thus, there exist apatites with different behaviour, non-resorbable and resorbable apatite (Watari *et al.* 2007*b*). It is necessary to know the effect of nanosizing on this change of biofunctions using nanoapatite composites (Liao *et al.* 2005, 2007*a*–*c*; Gelinsky *et al.* 2007; Li *et al.* 2008*a*).

1.5. Carbon nanotubes

As another typical subject of nanomaterials, much attention has been paid to carbon nanotubes (CNTs) up to now owing to their unique structure (Asakura *et al.* 2005; Ushiro *et al.* 2006) and properties. The development of applications in the electronic and chemical fields such as field emission electron gun and hydrogen storage materials has been intensive. Recently, the derivatives of CNTs with different structures and compositions have also been discovered and synthesized (Sato *et al.* 2005*a*). Nanomaterials (Watari *et al.* 2007*a*,*b*, 2008*b*) and nanocomposites (Liao *et al.* 2007*d*) may have various effects on living organisms. There are arguments that CNTs may have serious toxicity due to their acicular or fibrous particle shape, associated with lung carcinogenicity of asbestos (Takagi *et al.* 2008). As an element, carbon (C) is bioinert. Graphite is used as an artificial heart valve due to its antithrombogenicity for biomedical application. There have not been many studies of CNTs and their biological effects (Kiura *et al.* 2005; Sato *et al.* 2005*a*,*b*; Yokoyama *et al.* 2005*a*) and biomedical applications (Fugetsu *et al.* 2004*a*,*b*; Akasaka & Watari 2005, 2008, 2009; Akasaka *et al.* 2005, in press *a*,*b*; Rosca *et al.* 2005; Uo *et al.* 2005*a*; Wang *et al.* 2005, 2007; Li *et al.* 2008*b*,*c*). From the viewpoints of both nanotechnology application and risk assessment of nanotoxicology, it is necessary to study the effect of nanosizing carbon by comparing isomorphs of macroscopic graphite and nanocrystalline CNTs.

1.6. Nanoparticle internal diffusion and drug delivery systems

Particles less than 10 μm can pass through the bronchial, and even smaller nanosize particles may reach the alveoli of lung. Then there is the possibility that the uptake of nanoparticles occurs through the respiratory system and the digestive system. Meanwhile drug delivery systems (DDS) are one of the most typical biomedical applications of nanoparticles being developed (Rosca *et al.* 2004). DDS is expected for the selective administration of anti-cancer agent and gene transfection to the desired organs. It is necessary to investigate the behaviour of nanoparticles in the internal body for the assessment of nanotoxicology and also essential to comprehend the diffusion paths of the DDS (Moller *et al.* 2008) to reach the diseased target (Chan *et al.* 2002; Moller *et al.* 2007; Smith *et al.* 2008). In this sense, internal diffusion is significant for both the demerit and merit aspects of nanotechnology.

1.7. Purpose

Thus, nanosizing effect is involved with plural processes and sometimes causes different behaviour from macroscopic size to biocompatible materials. This strongly suggests the necessity to reveal the micro/nanosizing effect of materials on the living organism. The present paper discusses the bioreaction of nanoparticles based on reviewing authors' past and additional data, where both biochemical cell functional tests and animal implantation tests investigated the micro/nanosizing effect and the dependence particle size on the reaction of cells and tissues. The behaviour of invading nanoparticles and internal diffusion inside the body was visualized using X-ray scanning analytical microscope (XSAM; Uo *et al.* 1999, 2001*a*,*b*, 2006) for the level of the whole body and organs (Watari *et al.* 2007*c*,*d*, 2008*a*). Then, the nanosizing effect on tissue regeneration and cell proliferation in apatite and CNTs was investigated, and the mechanism of the conversion of functions from those in macroscopic scale was discussed.

2. MATERIAL AND METHODS

2.1. Specimens

Various sizes of particles were used as specimens for 99.9 per cent pure Ti, Fe, Ni, TiO_2 and CNTs. For Ti and Fe, particles of nominal size from 500 nm to 150 μm were used. To reduce the size distribution as small as possible and equalize the experimental conditions among the materials of metallic Ti, Fe and Ni, the particles of 500 nm, 3 and 10 μm were extracted by sedimentation and those less than 300 nm were extracted by ultrafiltration from the particle group with the size distribution (Tamura, K. *et al.* 2002).

2.2. Dissolution test of Ti, Fe and Ni particles

After Ti, Fe and Ni particles were immersed in Hanks balanced salt solution (HBSS) at 37°C for one month, the supernatant was filtered through a 0.45 μm membrane to remove particles and then elemental analysis was done by inductively coupled plasma-atomic emission spectrometry (ICP-AES) using ICPS-8100, Shimazu, Tokyo, Japan.

2.3. Biochemical analyses of cellular reaction to materials

Particles smaller (500 nm and 3 μm) and larger (10, 50 and 150 μm) than neutrophils were used to determine the relationship between cells and particle size with respect to cytotoxicity.

Human neutrophils, which play a central role in the initial stage of inflammation against foreign bodies, were used as probe cells. Neutrophils were separated from human peripheral blood from healthy volunteers with 6 per cent isotonic sodium chloride containing the hydroxyethyl starch and lymphocyte isolation solution (Ficoll-Hypaque, Amersham Pharmacia Biotech AB, Sweden). After the particles were mixed with HBSS kept at 37°C and neutrophils were added, they were used for various cell toxicity tests. The human acute monocytic leukaemia cell line, THP-1 cell, was also used for additional experiments.

Cell survival rate, lactate dehydrogenase (LDH) values and superoxide anion (O^{2-}) production per 10^6 neutrophils were measured. Cytokines of tumor necrosis factor-α (TNF-α) and interleukin-1β (IL-1β) were measured using ELISA kits (Endogen, Inc. USA). Morphological change of neutrophils mixed with HBSS containing various particles was observed by optical microscopy (OM: Zeiss, Axioskop, Germany) and scanning electron microscopy (SEM: Hitachi S-4300, Tokyo, Japan) (Kumazawa *et al.* 2002; Tamura, K. *et al.* 2002).

2.4. Animal implantation experiments

Particles were inserted into the subcutaneous connective tissue in the abdominal region of Wistar rats aged between 11 and 12 weeks (weight 350–380 gf). Specimens were prepared through the usual process of fixation, embedding, sectioning, staining with haematoxylin–eosin and histopathological observation was performed.

2.5. Visualization of internal distribution of nanoparticles

The compulsory exposure test to the respiratory system was performed on rats using the TiO_2 particles of a nominal size 30 nm. The uptake of nanoparticles through the digestive system was also tested in mice by mixing agar gelatin containing 30 nm TiO_2 particles with their foods. To inspect internal diffusion more simply, the experiments were done for mice by injecting nanoparticles directly into the cardiovascular system to the caudal vein. The observation of the internal distribution of nanoparticles was conducted for the whole body and each organ by elemental mapping in air using XSAM (Horiba XGT-2000V, Tokyo, Japan) without the pre-treatments of fixation, dehydration and staining after sectioning. The distribution inside the organ was also inspected by elemental mapping using energy dispersive X-ray spectroscopy (EDS) installed to SEM. The experiments were also carried out for the particles Ti, Fe, Ni, Pt, TiO_2, TiC, Fe_3O_4, Fe_2O_3 and CNTs. Chemical analysis was done by ICP-AES for organs and compared with the results of XSAM mapping (Watari *et al.* 2007*c*,*d*, 2008*a*).

2.6. Biomimetic nanoapatite/collagen composite

HAP–collagen composites synthesized biomimetically on collagen type I were implanted into the subcutaneous tissue and bone defects in the femur of rats for 1–12 weeks and observed histopathologically (Yokoyama *et al.* 2005*b*).

2.7. CNTs

CNTs were used including single-wall CNTs (SWCNTs) of 0.9–1.5 nm in diameter and 2–3 μm in

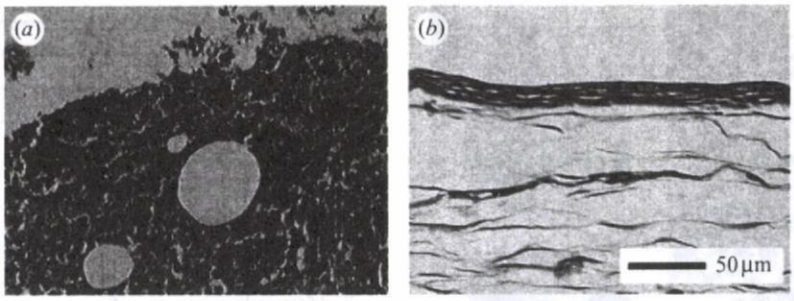

Figure 2. Histological image of rat soft tissue inserted with (*a*) Ni and (*b*) Ti implants of macroscopic size (1 mm $\phi \times 10$ mm) after one week (Watari *et al.* 2007*b*).

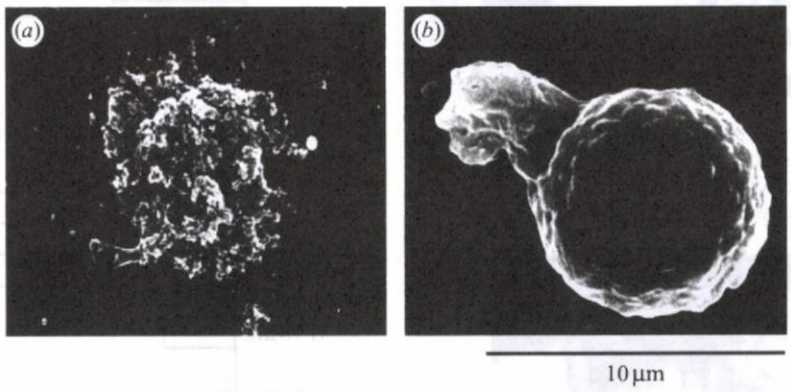

Figure 3. SEM images of human neutrophils exposed to the 500 nm particles of (*a*) Ni and (*b*) Ti (Watari *et al.* 2007*b*).

length synthesized by arc discharge method with a purity of 90 per cent (Meijo Nano Carbon Co., Ltd), multi-wall CNTs (MWCNT) of 5–20 nm in diameter and 20–40 μm in length synthesized by the chemical vapour deposition technique with a purity of 98 per cent (NanoLab, Inc., MA, USA) and carbon nanofibres for part of the experiments. In some cases, CNTs were purified by the removal of metal particle catalysts of Ni and Fe using acid agents such as hydrochloric acid and amorphous carbon by heating in air. By these treatments, CNTs gained some hydrophilicity. CNTs were dispersed in the deionized water by sonication for 3 min. Various nanotube (NT) scaffolds were made by vacuum filtration of the dispersed NT slurry onto porous polycarbonate (PC) membranes.

2.8. Cell culture

Human osteoblast-like cells (Saos2) were used for cell culture. Cells were cultured in Dulbecco's modified Eagle's medium (DMEM; SIGMA) with 10 per cent foetal bovine serum (FBS; Biowest) by the usual process. The morphology of cells was observed by OM, confocal laser scanning microscopy and SEM. The number of cells was counted from the SEM micrographs of those attached to each scaffold, since the detachment of cells from scaffold by trypsin could not be applied for CNT scaffolds. The adsorbed amount of proteins on each scaffold was measured using bicinchoninic acid protein assay reagent after immersion in the cell culture medium for 24 hours. Alkaline phosphatase (ALP) activity was measured with LabAssay ALP (Wako, Japan) for the cells cultured on each scaffold (Aoki *et al.* 2005, 2006, 2007*a*,*b*).

2.9. Observation and characterization

Morphology of particles and cells was observed by SEM, and elemental analysis by EDS was also carried out. The high resolution observation of CNT was done with the multi-beam high-voltage electron microscope (JEM-ARM-1300, JEOL, Japan) of the Center for Advanced Research of Energy Conversion Materials, Hokkaido University, at an accelerating voltage of 1250 kV.

Animal experiments were performed in accordance with the Guide for the Care and Use of Laboratory Animals, Hokkaido University Graduate School of Dental Medicine. During the course of this study, no rats were lost.

3. RESULTS

3.1. Soluble and non-soluble materials: reaction from macro to micro/nano

Figure 2 shows the comparison of tissue reaction to the macroscopic size (1 mm $\phi \times 10$ mm) of Ni (figure 2*a*) and Ti (figure 2*b*) after one week implantation in the dorsal thoracic region of rat. The implant had been situated in the upper space of each photograph. In Ni, the expansion of capillary vessels was observed. Tissue in the photograph was showed necrosis and degeneration in the distant region. For Ti, a fibrous connective tissue had already formed surrounding implants from the earlier stage, which is a feature of biocompatible materials.

Figure 3 shows the SEM image of human neutrophils exposed to the 500 nm particles of Ni (figure 3*a*) and Ti (figure 3*b*) in HBSS. The morphology of neutrophils exposed to Ni particles was often transformed or

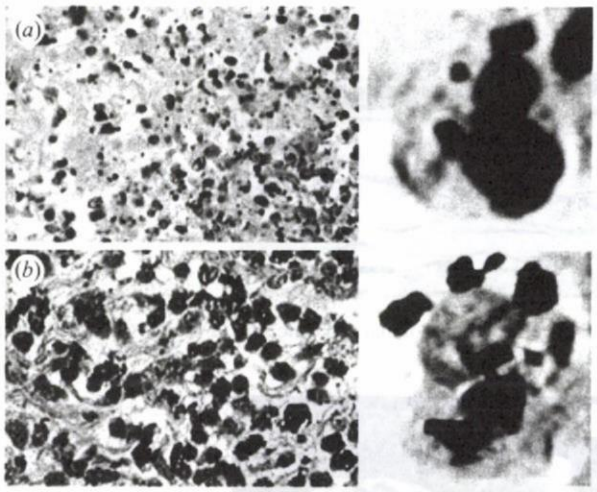

Figure 4. Histopathological observation of tissue reaction to the short-term implantation of the (*a*) 500 nm Ni and (*b*) 3 μm Ti particles. The enlargement of one cell is shown on the right. (*a*) Necrosis and (*b*) inflammation occurred, respectively.

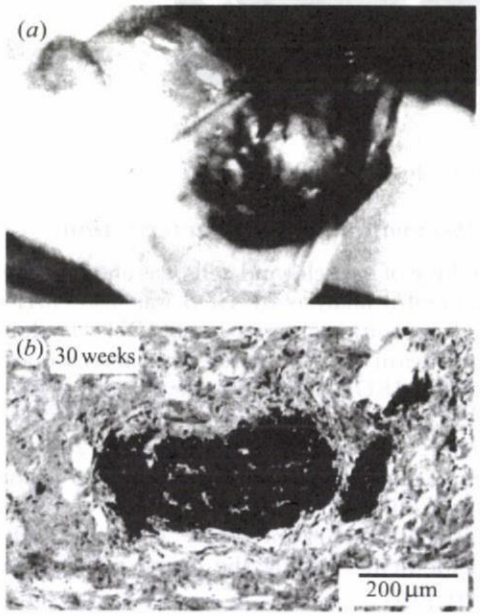

Figure 5. Tissue reaction for the long-term implantation to the (*a*) 500 nm Ni and (*b*) 3 μm Ti particles. Tumour was induced after 1 year implantation of the 500 nm Ni particles (Watari *et al.* 2007*b*).

destroyed due to its toxicity (figure 2*a*). For Ti (figure 2*b*), a neutrophil is extending its pseudopod and going to phagocytize a 500 nm Ti particle. For the particles larger than approximately 10 μm, phagocytosis was not observed.

Figure 4 shows the comparison of histopathological observation of tissue reaction to the short-term (5 days) implantation in the subcutaneous tissue of the rat for 500 nm Ni and 3 μm Ti particles. The enlargement of a single cell is shown on the right side. For Ni particles necrosis occurred, while Ti particles were phagocytized by macrophages and other giant cells.

Figure 5 showed the tissue reaction to the long-term implantation of the 500 nm Ni and 3 μm Ti particles. Figure 5*a* is a tumour induced after a 1-year implantation

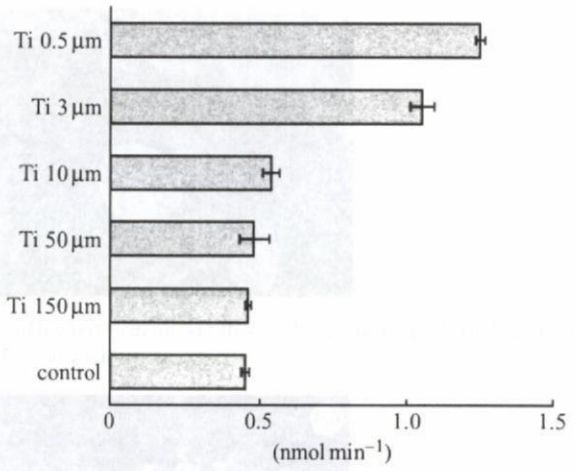

Figure 6. Dependence of superoxide production from neutrophils on Ti particle size (Tamura, K. *et al.* 2002).

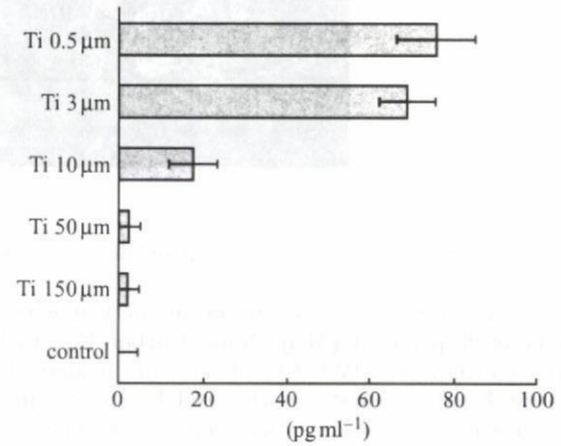

Figure 7. Dependence of IL-1β production from neutrophils on Ti particle size (Tamura, K. *et al.* 2002).

of Ni particles in the subcutaneous tissue of a rat. Ni is already toxic in macroscopic size as seen in figure 2. When fine particles, toxicity is enhanced remarkably. Figure 5*b* shows 3 μm Ti particles after 30 weeks. Particles had been dispersed more widely in tissue just after implantation. In the long term, they became gradually agglomerated by the biological processes of repeated cycles of phagocytosis and cell death.

3.2. Particle size dependence on cell/tissue reaction and function

Figures 6 and 7 show the released amount of superoxide and IL-1β from human neutrophils in HBSS mixed with the various sizes of Ti particles. IL-1β is one of the most representative cytokines of inflammation. HBSS was the control. Both superoxide and IL-1β were increased with the decrease in particle size. The increase was especially pronounced for 3 μm and 500 nm. The release of LDH showed similar behaviour, while cell survival rate showed the inverse decreasing tendency.

Figure 8 shows the dissolution from 3 and 10 μm particles of Ti (figure 8*a*), Fe (figure 8*b*) and Ni (figure 8*c*) analysed by ICP-AES. Under the conditions of figures 6 and 7, ICP elemental analysis indicated that the dissolution from Ti particles was

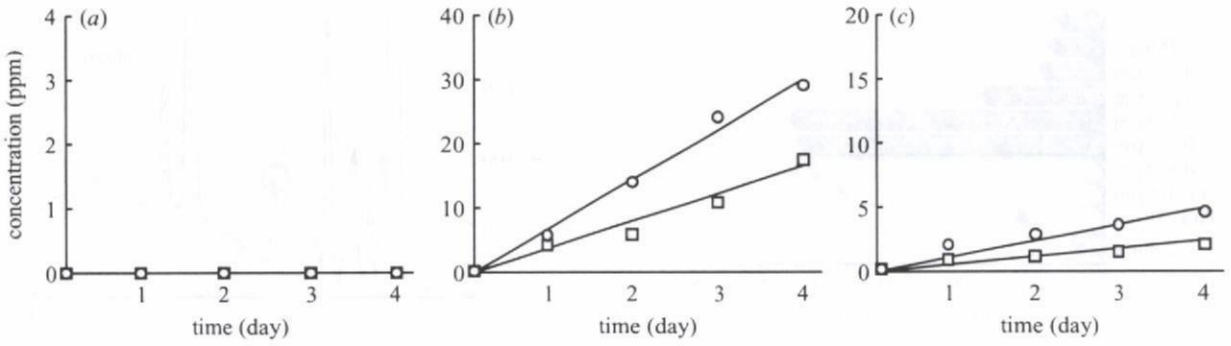

Figure 8. Dissolution from 3 μm (circles) and 10 μm (squares) particles of (*a*) Ti, (*b*) Fe and (*c*) Ni analysed by ICP-AES.

negligible below detection limit. This suggests that the pronounced phenomena of biochemical cell reaction seen below 10 μm in figures 6 and 7 are not due to the ionic dissolution effect.

For Fe and Ni, the dissolution amount depends on the particle size. The smaller 3 μm particles dissolve more than 10 μm particles. Fe is very soluble if we take the 10 times larger value of the vertical axis into account. The dissolution of Ni is smaller than Fe, but Ni shows a much more toxic effect as shown in figures 2–5.

Figure 9 shows the comparison of TNF-α release for Ti, Fe and Ni particles. TNF-α is another one of the most representative cytokines of inflammation as well as IL-1β. Ti and Fe showed the similar increasing tendency with the decrease in particle size. The increase was drastically pronounced for 3 μm particles. ICP results (figure 8) showed that the chemical properties of Ti and Fe particles are completely different. Ti is non-soluble and Fe is very soluble. Nevertheless, the effect of Fe is nearly equivalent to that of Ti even in a quantitative sense, although the chemical properties of each are very different.

Ni also showed the size dependence. However, the quantitative values are different from Ti and Fe. Ni showed the size dependence with the relatively lower values. The release of superoxide and IL-1β showed a tendency similar to that for Ti and Fe. Cell survival rate was much smaller than control (HBSS) and LDH was higher.

Figure 10 shows the histological image of rat tissue reaction to 3 μm (figure 10*a*) and 10 μm (figure 10*b*) Ti particles after 5 days of implantation in the soft tissue of rat. For the 3 μm Ti particles, phagocytosis by macrophages and inflammatory cells occurred, and Ti particles were observed in the cytoplasm of cells, whereas the 10 μm Ti particles were outside cells, phagocytosis was rarely observed and tissue was much less inflammatory. The size dependence *in vivo* observed in figure 10 resembles the results *in vitro* in figures 3*b* and 9, which suggests that TNF-α expression is closely related to the occurrence of phagocytosis.

The histological observation of rat tissue reaction to the implantation of different size of Ti particles 3, 10, 50 and 150 μm was carried out for up to 30 weeks. For the 150 μm Ti, each particle was surrounded by fibrous connective tissue layer, which is similar to the case of macroscopic Ti implant shown in figure 2*b*. Tissue reaction to the 10 μm Ti was inflammatory with inflammatory cell infiltration as well as fibrous

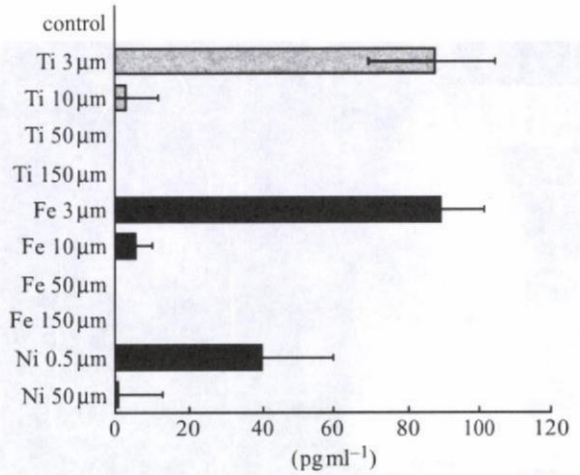

Figure 9. Dependence of TNF-α release from neutrophils on particle size for Ti, Fe and Ni (Watari *et al.* 2007*a*).

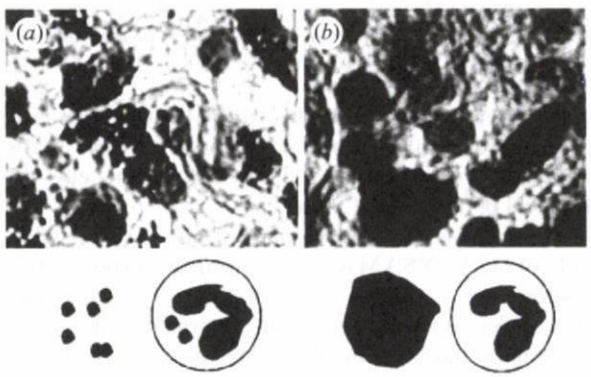

Figure 10. Tissue reaction of rat to (*a*) 3 μm and (*b*) 10 μm Ti particles after 5 day implantation (Watari *et al.* 2007*a*).

connective tissue formation. For the 3 μm Ti, the originally dispersed particles in tissue in short-term implantation became gradually agglomerated over time in the long term by the biological process of repeated cycles of phagocytosis and cell death. Weak inflammation continues chronically after 30 weeks.

3.3. Invasion and internal diffusion of nanoparticles

Figure 11 shows the dependence of TNF-α release from neutrophils on particle size down to the nm scale. Stimulus, represented as amount of TNF-α release, is

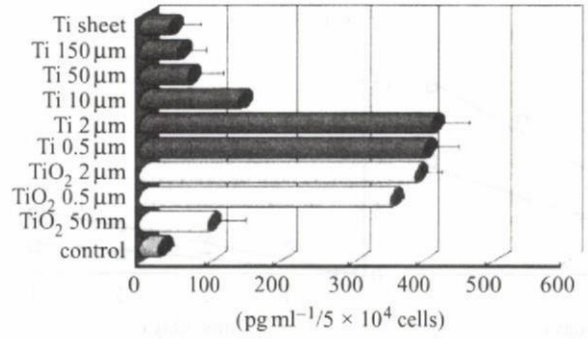

Figure 11. Dependence of TNF-α release from neutrophils on particle size down to the nm scale (Watari *et al.* 2007*a*).

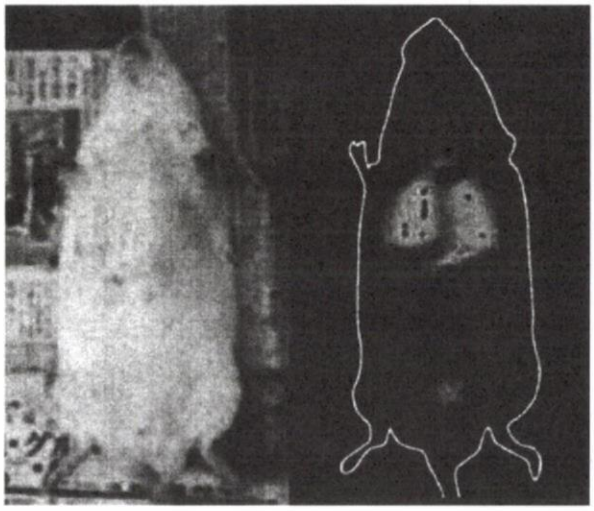

Figure 12. XSAM Ti mapping of internal distribution of the 30 nm TiO_2 particles after the compulsory exposure testing of the respiratory system (Watari *et al.* 2007*d*).

pronounced below 3 μm. It exhibited the maximum from approximately μm down to 500 nm. For smaller sizes, it decreased below 200 nm and became closer to the level of 50 μm and larger.

Figure 12 is the Ti mapping of the internal whole body of rats by XSAM after a compulsory exposure test. It shows the distribution of the 30 nm TiO_2 particles. The condensation occurred from the respiratory system to urinary bladder by diffusion in the whole body through the cardiovascular system after the direct uptake from pulmonary alveoli into blood vessels.

Figure 13 is the XSAM elemental analysis from the spleen for the case after 10 days of oral administration of 30 nm TiO_2 particles. Although peak height is small in this case, a Ti-Kα peak undoubtedly exists other than Fe-Kα peaks at approximately 6.5 keV and peaks of incident X-ray from Rh target below 4 keV. This confirms the phenomenon that nanoparticles were taken into the internal body through the digestion system.

Figure 14 shows the X-ray transmission image and the corresponding Ti elemental mapping by XSAM for 5 min, 3 hours and 1 day after injection of the 30 nm TiO_2 particles directly into the cardiovascular system of the mouse through the caudal vein. TiO_2 nanoparticles diffuse to the lung through the heart

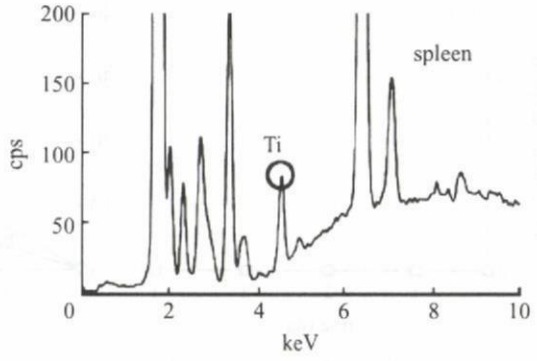

Figure 13. Elemental analysis of spleen of mouse by XSAM after oral administration of 30 nm TiO_2 particles for 10 days (Watari *et al.* 2008*a*).

from the caudal vein just after injection, then to the liver and further to the spleen with time.

3.4. Conversion of functions by nanosizing and HAP

Figure 15 shows an example of failure in a dental implant of HAP-coated titanium before (figure 15*a*) and after (figure 15*b*) implantation. Failures of dental implant occur for various reasons. One of the causes is the dust of apatite produced by dropout, exfoliation, delamination or abrasion. This induces inflammation and the resorption of newly formed bone and coated apatite.

The biomimetically synthesized nanocomposites of apatite and collagen fibrils are bioresorbable in the subcutaneous tissue. Then these nanoapatite composites were implanted in bone defects or bone marrow. Figure 16 shows the histopathological image when nanoapatite composites were implanted in the bone marrow of rat for eight weeks. Phagocytosis of composites by osteoclasts and osteogenesis by osteoblasts occurred simultaneously and adjacently to each other. The area of nanocomposites (asterisks) was decreased and covered with new bone (white asterisks) of lamellar structures. Resorption of the composites and replacement by new bone proceeded with time by 12 weeks. As a result, nanoapatite composites work as bone substitute materials for hard-tissue reconstruction.

3.5. Conversion of functions by nanosizing CNTs

Figure 17 shows the SEM image of osteoblast-like Saos2 cells cultured on graphite (figure 17*a*) and MWCNT (figure 17*b*) scaffolds for 7 days. Although graphite and CNTs are isomorphs of carbon and composed of graphene sheets that are similarly in crystal structure, they make a contrasting difference in the cell attachment and proliferation. Very few cells were attached to graphite (figure 17*a*), while many cells were attached to CNTs (figure 17*b*).

Cell growth cultured on CNTs showed the characteristic behaviour. Saos2 is usually grown in a spindle shape. On CNT scaffold, cells are grown fully to the whole direction with numerous fine filopodia at the cell edge.

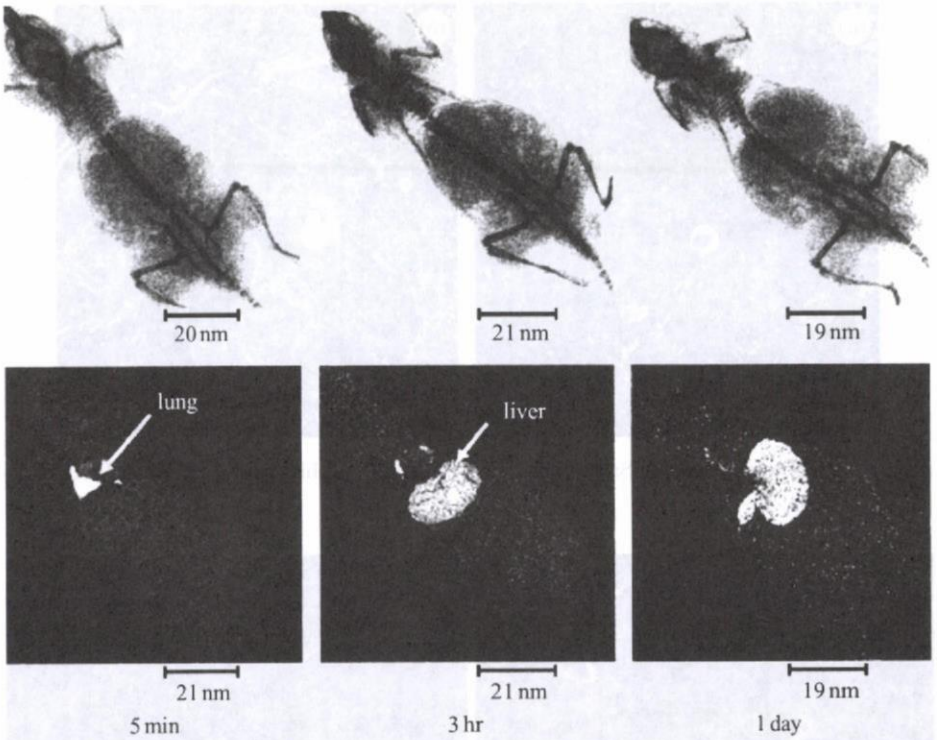

Figure 14. Time course of internal diffusion of the 30 nm TiO_2 particles after injection to the caudal vein, visualized by XSAM.

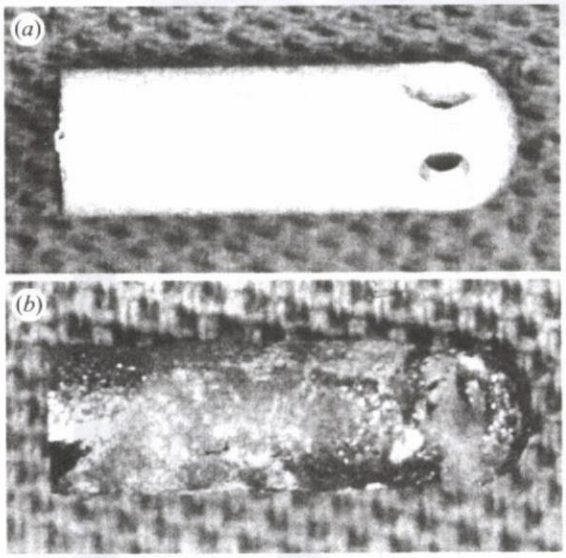

Figure 15. Example of failure in dental implant of apatite-coated titanium: (*a*) before and (*b*) after implantation.

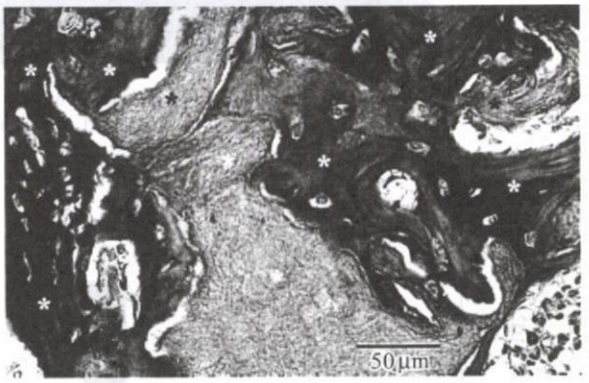

Figure 16. Histological image at eight weeks after implantation in the bone marrow of rat. Nanocomposites were resorbed (black asterisks) and partly replaced by new bone (white asterisks) with lamellar structures. AZ stain.

Figure 18 shows the SEM observation of the filopodia grown from the periphery of osteoblast-like cells on MWCNT scaffolds (figure 18*a*) and the enlarged image of the end of filopodium (figure 18*b*). Compared with usual cell culture, numerous filopodia are extended farther in the cell periphery (figure 18*a*) and combined with CNT meshwork. When trypsin, usually used to detach cells for cell number counting, was applied, cells would normally detach and float up, but could not separate from scaffold owing to the binding of filopodia with CNTs. These results show the high cell adhesiveness of CNTs.

Figure 19 shows the number of Saos2 cells cultured on the scaffolds of PC, graphite, MWCNT and SWCNT for 7 days. The cell numbers increased with culture time. However, cell number was nearly null on graphite, and the largest on SWCNTs of the four scaffolds, followed by MWCNTs.

Figure 20 shows the adsorbed amount of proteins on the scaffolds of PC, graphite, MWCNT and SWCNT when immersed in the cell culture medium for 24 hours. The amount of adsorbed protein is very low for graphite and the highest for SWCNT, followed by MWCNT.

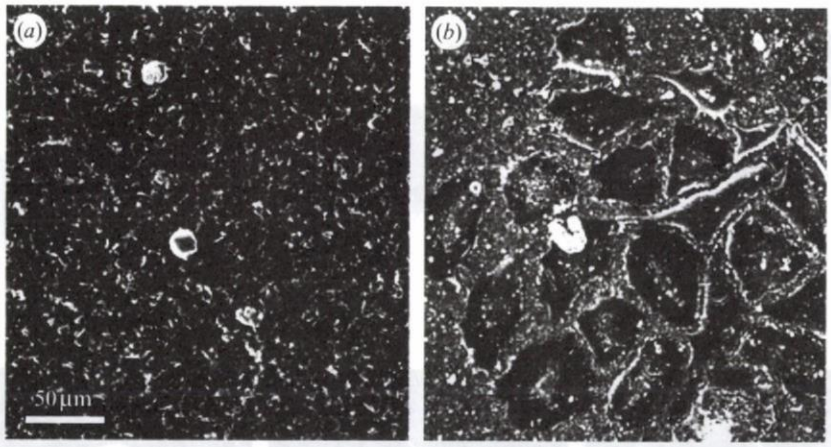

Figure 17. SEM image of osteoblast-like Saos2 cells cultured on (*a*) graphite and (*b*) MWCNT scaffolds for 7 days.

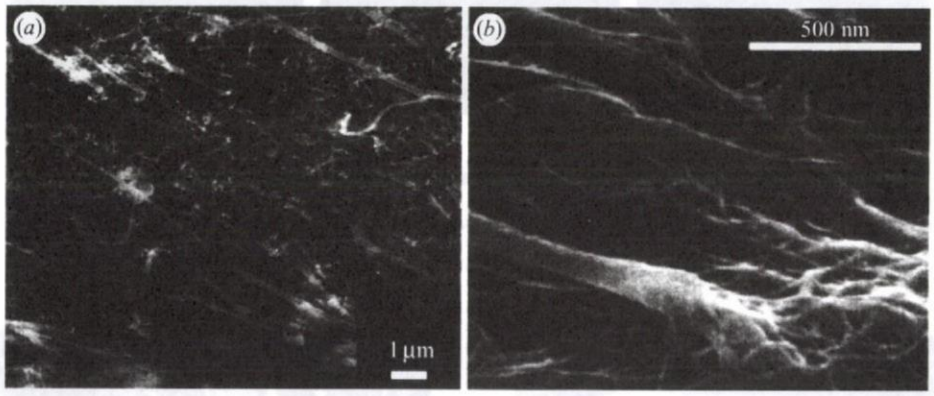

Figure 18. (*a*) SEM observation of filopodia grown from the periphery of osteoblast-like cells on MWCNT scaffolds and (*b*) the enlarged image of the end of filopodium.

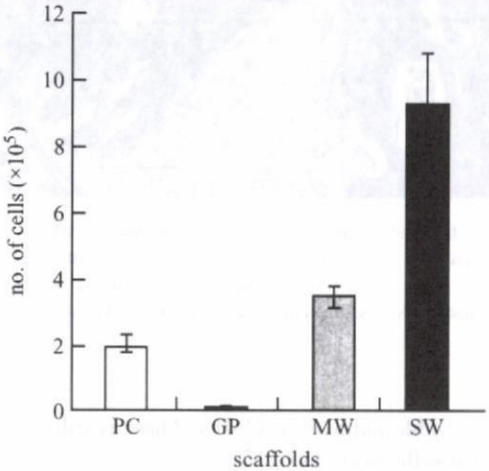

Figure 19. Number of Saos2 cells cultured on the scaffolds of PC, graphite (GP), MWCNT (MW) and SWCNT (SW) for 7 days.

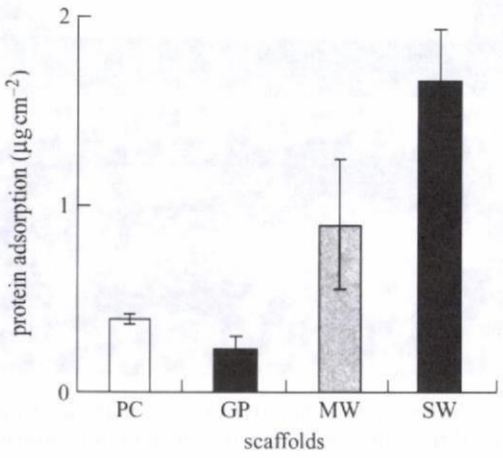

Figure 20. Adsorbed amount of proteins on the scaffolds of PC, graphite (GP), MWCNT (MW) and SWCNT (SW) in cell culture medium after 24 hours immersion (Aoki *et al.* 2007*a*).

Figure 21 is the expression of normalized ALP activity from osteoblast-like cells (Saos2) cultured on scaffolds of PC, graphite, MWCNT and SWCNT for 7 days. The degree of expression was very low for graphite, while it was increased remarkably in CNTs, the greatest increase in SWCNTs, then MWCNTs.

4. DISCUSSION

4.1. Soluble and non-soluble materials: effect on biocompatibility in macroscopic size

One of the most influential factors on biocompatibility of materials (Matsuno *et al.* 2001) is their dissolution

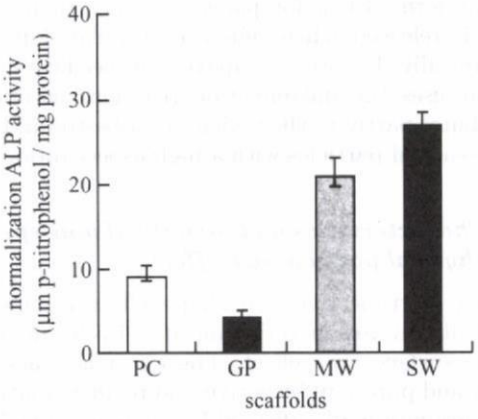

Figure 21. Expression of normalized ALP activity from Saos2 cells cultured on the scaffolds of PC, graphite (GP), MWCNT (MW) and SWCNT (SW) for 7 days.

properties. The interaction of materials with cells and tissue starts in most cases from ionic dissolution, whether it is nutrition intake or toxicity expression by poison. The toxicity effect may be evaluated as the degree of toxicity of materials×solubility. Corrosion resistance is, therefore, a prerequisite for biomaterials. This is the case for most of materials in a macroscopic size.

To compare the dependence of reaction of cells and tissue on the properties of materials with and without dissolution, Ni and Ti were selected as the representative metals for dissolvable, toxic metals and for non-dissolvable, biocompatible metals, respectively. Figures 2–5 showed the change of bioreaction to materials for the size from macroscopic to micro/nanometre. For macroscopic size, Ni (figure 2*a*) showed necrosis in the surrounding tissue of implant, while Ti (figure 2*b*) is encapsulated with fibrous connective tissue, which is the typical reaction of tissue to biocompatible materials (Uo *et al.* 2001*a*,*b*).

4.2. Nanosizing effect: specific surface area effect, the contribution of composition

The specific surface area increases in a reciprocally proportional manner to particle size. Therefore, the importance of dissolution properties becomes greater for micro- and nanosizes (downward direction in figure 1*a*) where the increase in specific surface area by nanosizing increases further chemical reaction, functions and toxicity. As shown in the *in vitro* cell reaction of figure 3, Ni caused the destruction of cells (neutrophils) (figure 3*a*) and Ti induced phagocytosis (figure 3*b*), when the size of materials became micro/nanometre (submicron).

As to the material dependence of cell toxicity that is, in other words, the effect of composition, the reaction similar to figure 3 *in vitro* also occurs *in vivo* as seen in figure 4 where necrosis occurred in cells and tissue for Ni nanometric particles. The results of figure 4 are those for the short term. The long-term implantation in tissue shown in figure 5 revealed that Ni particles generated a tumour after 1 year. This is the typical example of the specific surface area effect that leads to the enhancement of chemical dissolution and therefore toxicity. It has a serious influence, causing toxicity in many cases and is most commonly taken into account for nanosizing effect.

4.3. Nanosizing effect: physical size effect

For biocompatible materials such as Ti and TiO_2, particles below 10 μm cause phagocytosis to cells as shown *in vitro* to neutrophils (figure 3) and *in vivo* to macrophages mostly (figure 4), and weak inflammation to tissue in the short term (figure 4). For the particles larger than approximately 10 μm, phagocytosis was not observed. A similar phenomenon of size dependency was also observed *in vivo* as shown in figure 10 where the 3 μm Ti particles were phagocytized by macrophages or giant cells, while the 10 μm Ti particles remained outside the cells, phagocytosis was rarely observed and tissue was much less inflammed. In the long term (figure 5), the originally dispersed 3 μm particles were agglomerated after multiple repetitions of phagocytosis and cell death for 30 weeks. Tissue remained in a light chronic inflammation state.

This effect involved the biological reaction process between particles and cells/tissues (figure 1*b*), which is different from the case of Ni. These phenomena cannot be explained by the specific surface area effect (figure 1*a*), but understood as the different effect from the material properties of either toxicity or biocompatibility. It is the physical size and shape effect. To see the further details of this effect, *in vitro* biochemical cell functional testing was performed.

4.4. Particle size dependence in cell functions

Superoxide anions are released from intracellular organs and cell membranes when cells are stimulated. TNF-α and IL-1β are the representative cytokines of inflammation.

The production of superoxide anion (figure 6), cytokines IL-1β (figure 7) and TNF-α (figures 9 and 11) showed an increasing tendency with an decrease in particle size, and the amount was pronounced remarkably with 500 nm and 3 μm particles. SEM and OM observations (figures 3 and 10) showed that only the 500 nm and 3 μm particles in Ti group were phagocytized by neutrophils. Phagocytosis is difficult for the particle sizes 10, 50 and 150 μm to neutrophils of approximately 5–10 μm in diameter.

Similarly, the cell survival rate decreased and, with a strong corresponding relationship, the value of LDH, which is the indication of cell disruption, increased, as the particle size of Ti decreased from 150 μm down to 500 nm (Kumazawa *et al.* 2002; Tamura, K. *et al.* 2002).

All the results showed agreement in their size dependence and the size effect becomes more remarkable with a decrease in size and especially pronounced for sizes below cell size, which is closely related to the phagocytosis shown in figures 3 and 10.

ICP elemental analysis showed that the dissolution from Ti particles was below the detection limit and negligible (figure 8). Therefore, the biofunctional change detected in the present study did not result

from a chemical effect of Ti ions, but occurred by physical size effect of Ti particles.

Another evidence for physical effect is the particle size dependence of TNF-α for different materials, Ti and Fe, which are biocompatible or cause very little cell toxicity in the macroscopic size. Although the chemical properties are quite different, Ti is insoluble and Fe is soluble as shown in the ICP elemental analysis (figure 8), figure 9 showed nearly the same size dependency of TNF-α emission even in a quantitative sense. This indifference in cytotoxicity between Ti and Fe again strongly suggests that cytotoxicity of these Ti and Fe particles is not due to the chemical effect by dissolved ions but the physical size effect. Further study using other materials such as ceramics (TiO_2) and polymer (polylactic acid; PLA) showed similar particle size dependence, which suggests that these phenomena observed in biocompatible or bioinert materials are the non-specific, physical particle and shape effects, which occur independently of materials.

4.5. Critical size from bulk to particles for biological organisms

Our past *in vivo* implantation tests in the soft tissue of rats using various sizes of Ti particles showed that the particles larger than 150 μm were each surrounded by fibrous connective tissue and there was no inflammation (Kumazawa *et al.* 2002). This is the usual reaction for the biocompatible materials of a macroscopic size such as the bulk Ti implant. For less than 100 μm, the cell becomes stimulated gradually by the decrease in particle size, partly because of the mechanical and morphological factors such as irritation by needlepoint shape crystals or acute surface roughness structure onto the cell wall. It is partly the effect of IL-1β sensitivity to particle shape as discussed below in §4.6. Another reason may be that the size becomes too small to encapsulate each particle with fibrous connective tissue, and particles tend to be exposed directly to cells/tissue. Thus, for biological bodies, the object approximately larger than 100 μm behaves as macroscopic or non-bioreactive and that less than approximately 100 μm behaves as particles.

4.6. Particle shape effect

TNF-α and IL-1β are both representative cytokines of inflammation. Our past study compared the effect of different particle morphology on the expression of TNF-α and IL-1β, using the set of massive and acicular TiO_2 particles with the equivalent diametral size and longitudinal length of 3–10 μm, respectively. TNF-α showed the increase in emission below 10 μm in a similar manner for both massive and acicular crystals. For IL-1β, massive crystals showed similar dependence to the case of TNF-α, while acicular crystals showed nearly the same level for the sizes below and over 10 μm. This suggests that TNF-α and IL-1β represent the different nature of stimulus in inflammation (Watari *et al.* 1997). TNF-α is closely related to phagocytosis, while IL-1β reflects not only the stimulus by phagocytosis but also by particle shape such as acicular form. Even for particles larger than 10 μm, IL-1β is released when cells are stimulated physicomechanically by steeple apexes of needle crystals. This arouses the inflammation reaction cascade and contributes partly to the toxicity of asbestos and other needle shaped particles with a high aspect ratio.

4.7. Characteristics and toxicity of non-specific, physical particle size effect

Physical particle size and shape effect occurs non-specifically in any material and it is irrelevant to the specific surface area effect. The effect appears more clearly and purely in bioactive and bioinert materials, which are minimally affected by chemical dissolution effects. However, the absolute level of stimulation such as IL-1β (figure 7) and TNF-α (figures 9 and 11) by these particles is very low, as small as 1/1000 to 1/10000, compared with endotoxin or lipopeptide (Kiura *et al.* 2005; Watari *et al.* 2007*a*). Therefore, this would not cause serious problems in the short term and in small quantities. However, since it still induces phagocytosis in cells and inflammation in tissue *in vivo*, it leads to chronic inflammation in the case of a large amount and a long-term exposure. The most typical serious cases are osteolysis by abraded particles (Tamura, Y. *et al.* 2002*a*,*b*; Uo *et al.* 2005*b*, 2007; Zhu & Watari 2007) in artificial joint and mesothelioma in asbestos (Watari *et al.* 2006). The lifetime of an artificial joint is sometimes limited to less than 10 years by osteolysis following the inflammation induced by abraded particles. In asbestos, the phagocytosis of acicular particles by alveolar macrophages is insufficiently completed due to their large longitudinal length and non-biodegradability. This results in cell death, cytokine emission and another differentiation of phagocytes. The long-term repetition of this phagocytosis cycle leads to chronic inflammation with superoxide production to attack foreign objects. Superoxides also hurt the DNA of the biological organism itself and cause carcinogenesis when the accumulation of defects in DNA surpasses the certain threshold.

4.8. Competitive effects of composition and particle size

Macroscopic Ni inserted in soft tissue induced necrosis in the nearby periphery (figure 2*a*) and heavy inflammation in the distant region. XSAM analysis revealed that these toxicity levels are due to the concentration of dissolved Ni ions (Uo *et al.* 1999, 2001*a*,*b*, 2006). The strong toxicity of Ni is originated mainly from its dissolved ions. Ni also showed the particle size dependence in cell functional testing, but the values of TNF-α expression (figure 9) were lower than those of Ti and Fe, although Ni has a stronger toxicity. The significantly lower cell survival rate and higher LDH values revealed in the past study indicated that cell destruction occurred with higher probability by exposure to Ni particles as seen in figure 3*a*. The effect of cell death might surpass the stimulatory effect of Ni and suppress the emission of TNF-α.

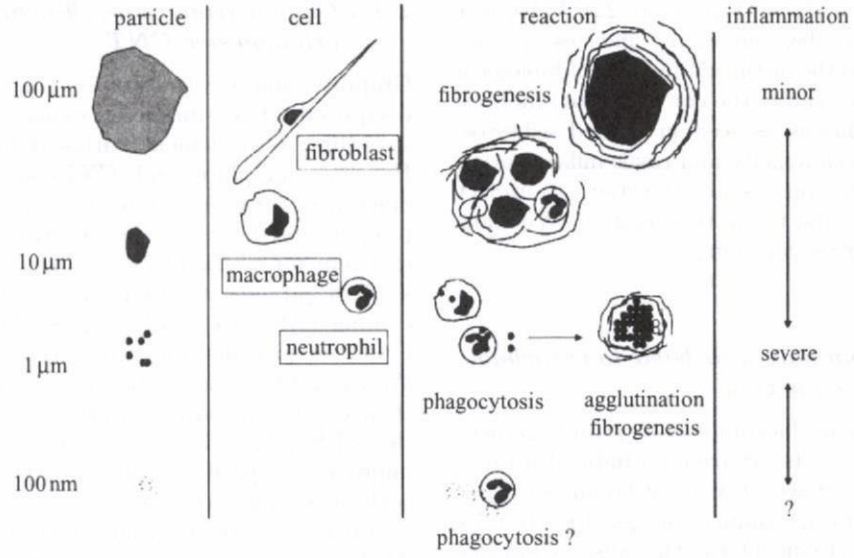

Figure 22. Origin of physical particle size effect: relationship between particle size and cell/tissue (Watari *et al.* 2007*a*).

In reality, most of the materials have some solubility. In those cases, both compositional effect, i.e. toxicity by surface area effect, and physical size effect appear by nanosizing. However, the chemical toxicity by specific surface area effect is far stronger and much more serious and acute, as shown in the case of Ni. Compared to this, the toxicity by physical particle size effect is regarded as nearly negligible (Kiura *et al.* 2005; Watari *et al.* 2007*a*). Therefore, for the soluble materials, both compositional and size effects appear, but size effect is negligible and compositional effect is dominant. For non-soluble or biocompatible materials, chemical ionic dissolution effect is negligible; therefore, pure physical particle size effect appears and becomes prominent.

4.9. Origin of particle size effect: relative size relationship with cells/tissue

The cell and tissue reaction changes from bulk to fine particles for the same material. Figure 22 shows the size relation between particle size and cells/tissues. The cell-stimulative and tissue-inflammatory nature of particles in the micro/nanorange originates from the relative size relationship with the cell/tissue (Watari *et al.* 2007*a*). The reaction inherent to the physical particle effect starts at approximately 100 µm and increases as size decreases. The micro/nanosizing of materials to below cell size makes them 'biointeractive' with cells and tissues (figure 1*b*) and leads to the conversion of functions through biological process as discussed below in §4.11. For less than 200 nm, stimulus diminishes towards the level of macro.

This is clearly distinguished from chemical reactivity enhancement effect by increase in a specific surface area (downwards in figure 1*a*). This originated solely from material properties to enhance greatly the same functions as those in the macroscopic size. Catalyst is a typical example of this effect and no biological interaction is involved.

4.10. Bioactive, biointeractive and bioreactive

Thus, the particles below cell size, approximately 10 µm become, we may say, biointeractive, since that size arouses phagocytosis in cells and inflammation to tissues irrespective of material type, and such a size can be 'biointeractable'. Usually, the term 'bioactive' is used for the nature to induce the intrinsic function of biological organism, in a positive sense to become merit for human beings. The typical example is HAP, which induces osteoconductivity and biocompatibility. However, merit or demerit is just the difference in evaluation system, whether they match the purpose of human beings or unintentionally appear to be against it. Irrespective of that, expression mechanisms stand on the same basis. If we generalize the meaning to the properties to induce the intrinsic function of biological organisms, whether it works as merit or demerit, micro/nano particles can be called bioactive in a more generalized sense. Since it is necessary to distinguish this from the usual use in a positive sense, we may use the word 'bioreactive' instead of bioactive for a more general meaning to induce the intrinsic function. Then we can say that micro/nanoparticles are bioreactive, where the size itself induces the reaction of biological body and may work both positively and negatively.

4.11. Conversion of functions by nanosizing through biological process

We have noted the phenomena of function conversion occurring by nanosizing for certain materials. The examples include the cases of Ti from its biocompatible nature in macroscale to inflammation, leading to osteolysis, in abraded micro/nanoparticles produced from an artificial joint and asbestos from a non-toxic composite of clay minerals (silicate) to carcinogenicity of mesothelioma in the needle-shaped nanoparticles. The mechanism involved in these conversions of function is based on the biological process of particle–cell/tissue interaction (figure 1*b*), originated

from a physical size relationship (figure 22). Whatever materials they may be, nanosizing induces a non-specific reaction and the intrinsic functions of biological organisms. This may lead to the conversion of functions under certain conditions as seen in Ti and asbestos. The bioreaction of cell toxicity and tissue inflammation develops through the conversion of functions to impact on cell proliferation and tissue regeneration. We show further examples in the following.

4.12. Change from non-resorbable to resorbable apatite by nanosizing

Apatite has excellent biocompatibility and induces new bone formation to its surface after implantation in bone circumstances. However, when it becomes micro/nanoparticles, apatite also induces phagocytosis to cells and inflammation to tissue. One of the causes of failures of dental implants is the dust or fine particles of apatite produced by dropout, exfoliation, delamination or abrasion. These induce inflammation in the periphery part of implant, which leads to the resorption of newly formed bone and coated apatite. This sometimes causes failures of dental implant as seen in figure 15. This is a similar type of conversion of functions as the case of abraded Ti particles.

Synthetic HAP exhibits excellent osteoconductivity in a macroscopic size, but it is not substituted for bone and remains permanently in the body. Therefore, it is suitable for use as an implant (Watari *et al.* 1997, 2004). Meanwhile, it is well known that natural bone is composed of collagen and nanoapatite crystallites of approximately 50 nm (Watari 2001, 2005). When the nanocomposites of apatite and collagen fibrils were biomimetically synthesized (Liao *et al.* 2005, 2007*a–c*; Gelinsky *et al.* 2007; Li *et al.* 2008*a*,*d*) and implanted in subcutaneous tissue, they were covered with fibrous connective tissue and then mostly resorbed in eight weeks by phagocytosis (Yokoyama *et al.* 2005*b*). Therefore, nanoapatite composites are bioresorbable.

When they were implanted in hard tissue situations such as bone defects or bone marrow, inflammation was induced, and osteoclasts and osteoblasts were then differentiated. Phagocytosis of nanoapatite composites by osteoclasts and osteogenesis by osteoblasts occurred simultaneously and adjacently to each other, as shown in figure 16. This tendency progressed with time and nanoapatite composites were finally replaced with new bone. The phenomena of resorption and bone formation were similar to the case of autologous bone graft. This process is also similar to the remodelling process of natural bone occurring constantly in our body (Yokoyama *et al.* 2005*b*). As a result, nanoapatite composites work as bone-substitute materials for hard-tissue reconstruction. Thus, nanosizing leads to another type of conversion of function from an osteoconductive, but non-bone substitutional nature in macro to bone substitutional properties in nano through a biologically induced process (Watari *et al.* 2008*c*).

4.13. Change from non-cell-adhesive graphite to cell adhesive CNT

Graphite and CNTs are isomorphs of carbon and composed of a similar graphene sheet in crystal structure. As an element, carbon (C) would be bioinert. However, graphite and CNTs show a contrasting difference in cell attachment (figures 17 and 18) and proliferation (figure 19), being very low for graphite and excellent for CNTs. CNTs adhere to collagen fibrils, a kind of protein, exposed on dentin surface by acid etching (Akasaka *et al.* in press *b*). This affinity of CNTs to proteins and also saccharides (Akasaka & Watari 2008) leads to the high adsorption of proteins (figure 20), including growth factors contained in the FBS added in the cell culture medium. This improves compatibility on the surface of CNTs, which is the basis for excellent cell adhesion (Akasaka *et al.* in press *a*), growth and functional expression of ALP activity (figure 20), a marker of osteogenesis capability (Aoki *et al.* 2007*a*; Li *et al.* 2008*b*,*c*). It is to be added that the precipitation of nanoapatite or calcium phosphate with a low crystallinity occurring in the simulated body fluid (SBF) also contributes to the improvement of biocompatibility (Akasaka & Watari 2005; Akasaka *et al.* 2005).

There are several factors that contribute to the affinity of CNTs to proteins. They include the similarity in composition, similarity in crystal structure, nanonetwork architecture in morphology, surface area, surface electronic charge and hydrophobic/hydrophilic properties. The hydrophobic interaction between carbon and proteins is generally counted for protein adsorption, but this could not explain the contrasting difference between graphite and CNTs, isomorphs of carbon, shown in figure 20.

The specific sites of adsorption of biological proteins in serum or tissue fluid are another matter of interest (Lundqvist *et al.* 2008). They are produced especially if CNTs are treated with acid or modified with some receptors. They provide more chemical and direct atomic binding between CNTs and proteins, which is important to create specific binding to particular targets. The existence of such sites is suggested from an experimental observation that the nucleation of acicular nanoapatite crystallites in SBF with added fluorine ions occurs radially from certain sites on CNTs (Akasaka *et al.* 2005). Although the contribution of specific sites is important, CNTs adsorb proteins even without such sites. The adsorption shown in this paper (figure 20) is mostly due to the more general, non-specific, physical adsorption. The nanometric curvature of graphene sheets composed of sixfold carbon rings in the tube atomic structure of CNTs generates a strong tendency to agglomerate by themselves and also an affinity to similar structures, one of which is protein.

Another factor that provides cell-adhesive properties is related to their structure. Although CNTs generally have a tendency to agglomerate and form bundles, the wavy and fibrous agglomeration still makes a nano-meshwork conformation with a large porosity where cells can take nutrient elements or growth factors easily.